Advances in Nano Research, *Vol. 9, No. 4 (2020) 237-250*
DOI: https://doi.org/10.12989/anr.2020.9.4.237

Free vibration and buckling analysis of elastically restrained FG-CNTRC sandwich annular nanoplates

Farzad Kolahdouzan[1], Mohammad Mosayyebi[2], Faramarz Ashenai Ghasemi[2], Reza Kolahchi*[3] and Seyed Rouhollah Mousavi Panah[4]

[1]*Faculty of Mechanical Engineering, University of Kashan, Kashan, Iran*
[2]*Faculty of Mechanical Engineering, Shahid Rajaee Teacher Training University, Tehran, Iran*
[3]*Institute of Research and Development, Duy Tan University, Da Nang 550000, Vietnam*
[4]*Faculty of Electronic Engineering, Shamsipour Technical and Vocational College, Tehran, Iran*

(*Received April 5, 2019, Revised April 9, 2020, Accepted September 29, 2020*)

Abstract. An accurate plate theory for assessing sandwich structures is of interest in order to provide precise results. Hence, this paper develops Layer-Wise (LW) theory for reaching precise results in terms of buckling and vibration behavior of Functionally Graded Carbon Nanotube-Reinforced Composite (FG-CNTRC) annular nanoplates. Furthermore, for simulating the structure much more realistic, its edges are elastically restrained against in-plane and transverse displacement. The nano structure is integrated with piezoelectric layers. Four distributions of Single-Walled Carbon Nanotubes (SWCNTs) along the thickness direction of the core layer are investigated. The Differential Quadrature Method (DQM) is utilized to solve the motion equations of nano structure subjected to the electric field. The influence of various parameters is depicted on both critical buckling load and frequency of the structure. The accuracy of solution procedure is demonstrated by comparing results with classical edge conditions. The results ascertain that the effects of different distributions of CNTs and their volume fraction are significant on the behavior of the system. Furthermore, the amount of in-plane and transverse spring coefficients plays an important role in the buckling and vibration behavior of the nano-structure and optimization of nano-structure design.

Keywords: buckling; free vibration; FG-CNTRC; sandwich annular nanoplate; elastically restrained edges

1. Introduction

Owing to striking characteristics of nanocomposites, these materials have been utilized in many essential fields including engineering and medicine and therefore, have received attentions amid scientists. Based on practical and theoretical investigations, various kinds of nanocomposites have been discovered which can be applied as reinforcements as well. Carbon Nanotubes (CNTs) are considered one of the well-known reinforcements and undoubtedly, using CNTs as reinforcement adds incredible benefits to the whole structures such as betterment of thermal and electrical conductivity, strength, stiffness and so on. This is why researchers initiated the investigation as to properties and advantages of nanocomposites (Vinson 1999, Herrmann *et al*. 2005) and mechanical behavior of structures reinforced by CNTs. Lei *et al*. (2013) carried out a buckling analysis of the FG-CNTRC plate based on the element-free Kp-Ritz approach. Results depicted the effect of the volume fraction of CNTs and the type of distributions on the behavior of the system. Wang *et al*. (2016) prepared semi-analytical solutions for the free-vibration and buckling analysis of the CNTRC thin plate. Also, the influences of CNTs and thermal environment were considered in this investigation. The zigzag vibration analysis of viscoelastic FG-CNTRC microplates bounded with piezoelectric layers was performed by Ghorbanpour-Arani *et al*. (2017). Ebrahimi and Habibi (2017) investigated the low-velocity impact response of laminated FG-CNTRC plates in thermal environment. In another paper, bending of FG-CNTRC plate which is rested upon elastic medium are analyzed by Zhang *et al*. (2015). Using First Order Shear Deformation Theory (FSDT), the structure is modeled mathematically and with respect to Ritz procedure, the nonlinear responses are achieved. Kiani (2017) carried out a research regarding dynamic behavior of FG-CNTRC cylindrical shell under moving force. In this work, various parameters including dispersion of CNTs, their volume fraction and boundary conditions and their influences upon mechanical behavior of structure have been assessed. It is indicated that rise of CNT volume fraction leads to reduction of dynamic response.

Besides FG-CNTRC structures having notable usages mentioned above, another form of structures named sandwich structures have substantial properties that can be utilized in various fields of engineering. Such properties can contain great strength to weight proportion, absorption of sound and vibration, great stiffness and light weight. So as to utilize them expeditiously, science of their either static or dynamic behaviors used in process of manufacturing would be essential. At the beginning, investigators carried out research as to mechanical properties (Van Vuure *et al*.

*Corresponding author, Ph.D.,
E-mail: rezakolahchi@duytan.edu.vn

ISSN: 2287-237X (Print), 2287-2388 (Online)

2000), failure (Gdoutos *et al*. 2002) and fatigue (Burman and Zenkert 2000) of sandwich structures. Further, Katariya *et al*. (2017) carried out a research about thermal buckling load of sandwich panel. In addition to obtaining and solving the governing equations using Higher order Shear Deformation Theory (HSDT) and Finite Element Method (FEM) respectively, influences of structural variables upon critical buckling load are discovered. Panda and Singh (2009) investigated post-buckling analysis of laminated shallow panel. The effects of lamination scheme and thickness ratio have been discussed. HSDT is utilized for obtaining the governing equations and the nonlinear FEM is used for solving these equations. Recently, in order to enhance properties of FG-CNTRC structures and spread its applications in another fields, utilizing sandwich structures and reinforcing them using CNTs are giving prominence. Vibration analysis of FG-CNT sandwich panel in thermal environment is conducted by Mehar and Kumar Panda (2018). HSDT is used for modeling mathematically and utilizing FEM, the governing equations are solved. Further, various kinds of CNT distributions and its effects on natural frequency of sandwich structure are analyzed. In another paper, nonlinear natural frequency of FG-CNT sandwich plate in thermal environment is analyzed by Mehar *et al*. (2017). Influence of thermal loads upon vibration of structure is discussed accurately. Moreover, FEM is used for solution of motion equations.

Smart structures in micro/nano scale is of interest of engineers due to their significant applications in medical science, aerospace engineering and robotic. In the past decades, nanotechnology and nanomaterials have undergone a rapid development in particular in micro/nano-electro-mechanical systems (MEMS/NEMS). With the improvement of MEMS and NEMS, the nonlocal theories have received great consideration. These theories can be listed as: Eringen theory, Modified Couple Stress Theory (MCST) and Strain Gradient Theory (SGT). It is worth mentioning that the nanostructures containing CNTs as reinforcement possess various applications such as transducers, solar cells, information storage and energy harvesting. Surface effects on scale-dependent vibration behavior of flexoelectric sandwich nanobeams was presented by Ebrahimi *et al*. (2019). In this paper, the flexoelectric effect on the mechanical properties of vibration piezoelectric sandwich nanobeam with different boundary conditions is investigated. Furthermore, Ghorbanpour-Arani *et al*. (2018) presented the size dependent buckling analysis of magnetoelectroelastic sandwich nanoplate. Thai and Vo (2012) discussed bending, buckling as well as vibration related to nanobeams using Sinusoidal Shear Deformation Beam Theory (SSDBT). Moreover, Karami *et al*. (2018) investigated Galerkin's approach for buckling analysis of functionally graded anisotropic nanoplates/different boundary conditions. George *et al*. (2019) analyzed and reviewed the polymers in nanoscale for the sake of drug delivery. They declared that using smart nanoparticles are able to enhance bio-availability, biocompatibility, time and so on. In another work, vibration control of nanobeam is investigated by Yue *et al*. (2019).

The LW theory is an amended theory accounting for thickness influences with minimum computational cost. Despite resemblance to single-layer theories, this theory hypothesizes discrete displacement field expansions within every subdivision. Indeed, the LW theory establishes a kinematically accurate demonstration of the strain field in separate layers. The analysis of static deformations and vibration of composite and sandwich structures based on LW theory and Radial Basis Functions and Pseudospectral (RBF-PS) method with an optimal shape parameter were performed by Ferreira *et al*. (2008). Furthermore, Alipour and Shariyat (2017) completed the free-vibration analysis of circular sandwich composite plates made with auxetic cores based on the LW theory. Results were compared with the 3D theory of elasticity extracted from ABAQUS, indicating the accuracy of the results of this theory. Moreover, Hajmohammad *et al*. (2018) carried out a LW theory for buckling analysis of truncated conical shells reinforced by CNTs and carbon fibers integrated with piezoelectric layers in hygrothermal environment.

So far, a research emphasizing LW theory for assessing vibration as well as buckling of FG-CNTRC sandwich nanoplate elastically restrained and covered by piezoelectric face sheets has not been studied. In fact, LW theory is able to hypothesize discrete displacement field expansions within every subdivision and its advantage is deriving accurate results for sandwich structures. Further, in this paper, various combination of non-classical boundary conditions and the effect of in-plane and transverse spring coefficients are analyzed for simulating this structure more realistic. The equations of motions are obtained using Hamilton's principle and solved using DQM. Meanwhile, the nonlocal elasticity theory is utilized to consider the small-scale effect. Various parameters such as the effects of nonlocal parameter, different types of FG distributions of CNTs, volume fractions of CNTs, stiffness coefficients of in-plane and transverse restraining spring on the natural frequency and critical buckling load of FG-CNTRC piezoelectric sandwich annular nanoplates are elucidated.

2. Formations

2.1 Nonlocal piezoelasticity theory

According to the nonlocal piezoelasticity theory, the stress field and electric displacement at one situation are related not only to the strains and electric component in the same situation of the body, but also to the strain in all other situations. The nonlocal constitutive equations of the piezoelectric material can be expressed as (Eringen 1983, Ghorbanpour Arani *et al*. 2017)

$$\sigma_{ij}^{nl}(x) = \int_V (|x - x'|, \tau)\, \sigma_{ij}^{l} dV(x') \qquad \forall x \in V \quad (1a)$$

$$D_k^{nl}(x) = \int_V (|x - x'|, \tau)\, D_k^{l} dV(x') \qquad \forall x \in V \quad (1b)$$

where σ_{ij}^{l} and σ_{ij}^{nl} represent local and nonlocal stress

tensors, respectively; D_k^l and D_k^{nl} represent the components of local and nonlocal electric displacement, respectively; $\lambda(|x-x'|, \tau)$ is the nonlocal modulus, $|x-x'|$ is the Euclidean distance, and $\tau = e_0/l$ describes the material constant where l is the external characteristic length, a is the internal characteristic length, and e_0 is Eringen's nonlocal parameter. Thus, for the two-dimensional instance, the constitutive equation of the nonlocal elasticity can be given as follows

$$(1-\mu\nabla^2)\sigma_{ij}^{nl} = \sigma_{ij}^{l} \tag{2a}$$

$$(1-\mu\nabla^2)D_k^{nl} = D_k^{l} \tag{2b}$$

in which parameter $\mu = (e_0 a)^2$ is the small scale effect and ∇^2 is the Laplacian operator.

2.2 Material properties of FG-CNTRC

In this study, it is supposed that the core layer of the sandwich annular plates is reinforced by SWCNTs as a reinforcement and the Poly-Para-Phenylene copolymer (PPP) is a matrix. CNT reinforcement is either uniformly (UD) distributed or FG along the thickness direction (z-axis). Three various types of FG distribution including $FG-A$, $FG-X$ and $FG-O$ types are considered. For each type of distribution, CNTs volume fractions can be mathematically written as (Shen 2009)

$$UD:\ V_{cnt} = V_{cnt}^* \tag{3a}$$

$$FG-A:\ V_{cnt} = \left(1-2\frac{z}{h}\right)V_{cnt}^* \tag{3b}$$

$$FG-X:\ V_{cnt} = 4\frac{|z|}{h}V_{cnt}^* \tag{3c}$$

$$FG-O:\ V_{cnt} = 2-4\frac{|z|}{h}V_{cnt}^* \tag{3d}$$

where

$$V_{cnt}^* = \frac{W_{cnt}}{W_{cnt} + (\frac{\rho^{cnt}}{\rho^m})(1-W_{cnt})} \tag{4}$$

in which W_{cnt} is the mass fraction of CNTs, ρ^{cnt} and ρ^m denote the densities of CNT and matrix, respectively. Based on rule of mixture (ROM), the effective material properties of the CNTRC nanoplates can be written as (Shen 2009)

$$E_{11} = \eta_1 V_{cnt}E_{11}^{cnt} + V_m E^m \tag{5a}$$

$$\frac{\eta_2}{E_{22}} = \frac{V_{cnt}}{E_{22}^{cnt}} + \frac{V_m}{G^m} \tag{5b}$$

$$\frac{\eta_3}{G_{12}} = \frac{V_{cnt}}{G_{12}^{cnt}} + \frac{V_m}{G^m} \tag{5c}$$

where V_m and V_{cnt} describe the volume fractions of the isotropic matrix and CNTs, respectively, related by $V_m + V_{cnt} = 1$. Meanwhile, E_{11}^{cnt}, E_{22}^{cnt} and G_{12}^{cnt} represent Young's moduli and shear modulus of orthotropic SWCNTs, respectively. E^m and G^m show the corresponding properties of the isotropic matrix. Furthermore, $\eta_i\,(i = 1, 2, 3)$ represents the efficiency factors of CNTs and is calculated from molecular dynamics (MD) simulations. The Poisson's ratio, ν_{12}, and the density of the nano composite plates, ρ can be written as (Shen 2009)

$$\upsilon_{12} = V_{cnt}^*\upsilon_{12}^{cnt} + V_m\upsilon^m \tag{6a}$$

$$\rho = V_{cnt}\rho^{cnt} + V_m\rho^m \tag{6b}$$

where υ_{12}^{cnt} and υ^m are Poisson's ratios of CNTs and matrix, respectively.

2.3 LW theory

A schematic configuration of FG-CNTRC annular nanoplates bounded with piezoelectric layers and edges elastically restrained by in-plane and transverse springs is depicted in Fig. 1. Moreover, in this figure, the four types of distributions of CNTs in the nanostructure such as *UD*, $FG-A$, $FG-X$ and $FG-O$ are illustrated.

The thickness of the top face sheet, core, bottom face sheet, and the total thickness of the structure are indicated by h_1, h_2, h_3 and h_t, respectively. Inner and outer radii are assumed r_i and r_o, respectively. Three transverse local coordinates which are taken as a reference in the middle of each layer are denoted for the top face sheet ($z^{(1)}$), core ($z^{(2)}$), and bottom face sheet ($z^{(3)}$), as are illustrated in Fig. 1. Boundary conditions are simulated by in-plane and transverse springs (k_u^i, k_u^o, k_w^i and k_w^o) along the inner and outer edges. It should be noted that different combinations of the classical boundary conditions can be easily simulated as some special types by setting correct spring stiffness. According to Zigzag sandwich Plate Theory (ZPT), the radial displacement component may be imagined as the result of the superposition of the global and local effects. Subsequently, by applying linear local displacement and global fields and by imposing kinematic continuity conditions in the connection position between layers, the LW displacement fields of the sandwich plates can be expressed as follows (Alipour 2016, Ferreira *et al.* 2008)

$$U^{(1)} = u_0 + z^{(1)}\theta_r^{(1)} + \frac{h_1}{2}\theta_r^{(1)} + \frac{h_2}{2}\theta_r^{(2)} \quad -\frac{h_1}{2} \le z^{(1)} \le \frac{h_1}{2} \tag{7a}$$

$$U^{(2)} = u_0 + z^{(2)}\theta_r^{(2)}, \qquad -\frac{h_2}{2} \le z^{(2)} \le \frac{h_2}{2} \tag{7b}$$

$$U^{(3)} = u_0 + z^{(3)}\theta_r^{(3)} + \frac{h_3}{2}\theta_r^{(3)} + \frac{h_2}{2}\theta_r^{(2)} \quad -\frac{h_3}{2} \le z^{(3)} \le \frac{h_3}{2} \tag{7c}$$

$$W = w_0 \tag{7d}$$

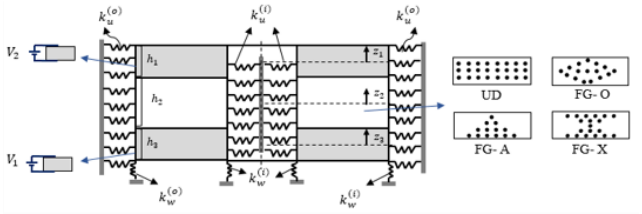

Fig. 1 FG-CNTRC piezoelectric sandwich annular nanoplate for four different type of CNTs distribution with edges elastically restrained

in which u_0 and w_0 respectively describe the radial and transverse displacement of the mid-plane of each plate, and θ_r^k (k = 1, 2, 3) represents the local rotation of the k^{th} layer. The strain components of any point of the sandwich annular structure in the cylindrical coordinate system are defined as

$$\varepsilon_r^k = \frac{\partial U^k}{\partial r} \tag{8a}$$

$$\varepsilon_\theta^k = \frac{U^k}{r} \tag{8b}$$

$$\varepsilon_{rz}^k = \frac{\partial U^k}{\partial z} + \frac{\partial W}{\partial r} \tag{8c}$$

The constitutive equation for stresses σ and flux density D for each layer of the sandwich annular plates can be expressed as (Ansari *et al*. 2017, Reddy 1984)

$$\begin{Bmatrix}\sigma_r\\ \sigma_\theta\\ \sigma_{rz}\end{Bmatrix}^k = \begin{bmatrix}Q_{11} & Q_{12} & 0\\ Q_{21} & Q_{22} & 0\\ 0 & 0 & Q_{44}\end{bmatrix}^k \begin{Bmatrix}\varepsilon_r\\ \varepsilon_\theta\\ \gamma_{rz}\end{Bmatrix}^K - \begin{bmatrix}0 & e_{31}\\ 0 & e_{32}\\ e_{15} & 0\end{bmatrix}^k \begin{Bmatrix}E_r\\ E_z\end{Bmatrix}^k \tag{9a}$$

$$\begin{Bmatrix}D_r\\ D_z\end{Bmatrix}^k = \begin{bmatrix}0 & 0 & e_{15}\\ e_{31} & e_{32} & 0\end{bmatrix}^k \begin{Bmatrix}\varepsilon_r\\ \varepsilon_\theta\\ \gamma_{rz}\end{Bmatrix}^k + \begin{bmatrix}\epsilon_{11} & 0\\ 0 & \epsilon_{33}\end{bmatrix}^k \begin{Bmatrix}E_r\\ E_z\end{Bmatrix}^k \tag{9b}$$

where

$$\begin{aligned} Q_{11}^k &= \frac{E_{11}^k}{1-\upsilon_{12}\upsilon_{21}}, \qquad Q_{22}^k = \frac{E_{22}^k}{1-\upsilon_{12}\upsilon_{21}}\\ Q_{12}^k &= \frac{\upsilon_{21}E_{11}^k}{1-\upsilon_{12}\upsilon_{21}}, \qquad Q_{44}^k = \frac{E_{11}^k}{2(1+\upsilon_{12})} \end{aligned} \tag{10}$$

Here, E_{11}^k and E_{22}^k are effective Young's moduli of each layer, and Q_{44}^k is the shear moduli and ν describes the Poisson's ratios. In Eqs. (9a) and (9b), e_{ij} (ij = 15, 31, 32) represents piezoelectric coefficients, and ϵ_{11} and ϵ_{33} are dielectric coefficients, respectively. Therefore, E_r and E_z are electric fields and can be described as follows (Ke *et al*. 2015)

$$E = -\nabla\emptyset \tag{11}$$

where the electric potential (Ø) is approximately supposed as a combination of cosine and linear variation. A distribution of the electric potential that satisfies the Maxwell equation for the annular nanoplates model is hypothesized as follows (Ke *et al*. 2015)

$$\emptyset^{(1)}(r,\theta,z,t) = -\cos\left(\frac{\pi z^{(1)}}{h_1}\right)\varphi^{(1)}(r,\theta,t) + \frac{2z^{(1)}V_0}{h_1} \tag{12a}$$

$$\emptyset^{(3)}(r,\theta,z,t) = -\cos\left(\frac{\pi z^{(3)}}{h_3}\right)\varphi^{(3)}(r,\theta,t) \tag{12b}$$

where $\varphi^{(k)}(r,\theta,t)$ is the spatial and variation of the electric potential in the mid-plane of the face sheets of the annular nanoplates and V_0 describes the external voltage.

3. Formulations

Hamilton's principle can be written as follows (Motezaker *et al*. 2020, Motezaker and Eyvazian, 2020)

$$\int_{t_0}^{t_1}[\delta U - \delta W - \delta K]\,dt = 0 \tag{13}$$

in which δU, δW and δK are the variations of strain energy, external works and kinetic energy, respectively. The elastic strain energy for the FG-CNTRC piezoelectric sandwich annular nanoplates can be expressed as (Alipour 2016)

$$\begin{aligned}\delta U = &\int_V (\sigma_r\delta\varepsilon_r + \sigma_\theta\delta\varepsilon_\theta + \tau_{rz}\delta\gamma_{rz} - D_r\delta E_r - D_z\delta E_z)\,rd\theta drdz\\ &+\int_{\Gamma_i} k_w^i\, w\delta w rd\theta + \int_{\Gamma_o} k_w^o\, w\delta w rd\theta\\ &+\int_h\int_{\Gamma_i} k_u^i\left(U^{(k)}\delta U^{(k)}\right)rd\theta dz^{(k)}\\ &+\int_h\int_{\Gamma_o} k_u^o\left(U^{(k)}\delta U^{(k)}\right)rd\theta dz^{(k)}\end{aligned} \tag{14}$$

where k_w^i, k_w^o, k_u^i and k_u^o show the stiffness coefficients of in-plane and transverse restraining spring, respectively, and Γ_i and Γ_o denote the inner and outer edges of the plates. The total kinetic energy of the FG-CNTRC piezoelectric sandwich annular nanoplates can be written as (Hosseini Hashemi *et al*. 2010)

$$K = \frac{1}{2}\left(\int_{r_i}^{r_o}\int_0^{2\pi}\int_{-\frac{h_t}{2}}^{\frac{h_t}{2}}\rho^k\left\{\left(\left(\dot{U}^k\right)^2 + \left(\dot{W}\right)^2\right)\right\}\right)rdrd\theta dz^{(k)} \tag{15}$$

Also, the applied external work can be written as follows

$$W = \frac{1}{2}\int_{r_i}^{r_o}\int_0^{2\pi}\left(N_e\left(\partial^2 w/\partial r^2 + 1/r\,\partial w/\partial r\right)\right)rdrd\theta \tag{16}$$

where N_e denotes the electric force (N_e = $2e_{31}V_0$). Substituting Eqs. (14)-(16) into Eq. (13), the governing equations in the cylindrical coordinate system (r,θ,z) can be written as

$$\delta u_0 : \left(N_r^{(3)} - N_\theta^{(3)}\right)/r + \partial N_r^{(3)}/\partial r + \left(N_r^{(2)} - N_\theta^{(2)}\right)/r \tag{17a}$$

$$+\ \partial N_r^{(2)}/\partial r+\left(N_r^{(1)}-N_\theta^{(1)}\right)/r+\partial N_r^{(1)}/\partial r$$
$$=(1-\mu\nabla^2)\times\left(\left(I_0^{(3)}+I_0^{(2)}+I_0^{(1)}\right)\times\partial^2u_0/\partial t^2+\left(I_0^{(1)}(h_1/2)+I_1^{(1)}\right)\partial^2\theta_r^{(1)}/\partial t^2+I_1^{(2)}\,\partial^2\theta_r^{(2)}/\partial t^2+\left(I_1^{(3)}-I_0^{(3)}(h_3/2)\,\partial^2\theta_r^{(3)}/\partial t^2\right)\right) \quad (17a)$$

$$\delta\theta_r^{(1)}\colon (h_1/2)\left(\left(N_r^{(1)}-N_\theta^{(1)}\right)/r+\partial N_r^{(1)}/\partial r\right)+\partial M_r^{(1)}/\partial r-R_{rz}^{(1)}=(1-\mu\nabla^2)\times\left(\left(I_0^{(1)}(h_1/2)+I_1^{(1)}\right)\partial^2u_0/\partial t^2+(h_2/2)\left((h_2/2)I_0^{(1)}+I_1^{(1)}\right)\partial^2\theta_r^{(2)}/\partial t^2+\left[I_2^{(1)}+h_1I_1^{(1)}+(h_1/2)^2I_0^{(1)}\right]\partial^2\theta_r^{(1)}/\partial t^2\right) \quad (17b)$$

$$\delta\theta_r^{(2)}\colon (h_2/2)\left(\left(N_r^{(1)}-N_\theta^{(1)}\right)/r+\partial N_r^{(1)}/\partial r\right)-(h_2/2)\left(\left(N_r^{(3)}-N_\theta^{(3)}\right)/r+\partial N_r^{(3)}/\partial r\right)+\left(M_r^{(1)}-M_\theta^{(1)}\right)/r+\partial M_r^{(2)}/\partial r-R_{rz}^{(2)}=(1-\mu\nabla^2)\times\left(\left((h_2/2)\,I_0^{(1)}+I_1^{(2)}-(h_2/2)I_0^{(3)}\right)\partial^2u_0/\partial t^2+(h_2/2)\left(I_1^{(1)}+(h_1/2)I_0^{(1)}\right)\partial^2\theta_r^{(1)}/\partial t^2-(h_2/2)\left(I_1^{(3)}-(h_3/2)I_0^{(3)}\right)\partial^2\theta_r^{(3)}/\partial t^2+\left[(h_2/2)^2\left(I_0^{(2)}+I_0^{(3)}\right)+I_2^{(2)}\right]\partial^2\theta_r^{(2)}/\partial t^2\right) \quad (17c)$$

$$\delta\theta_r^{(3)}\colon -(h_3/2)\left(\left(N_r^{(3)}-N_\theta^{(3)}\right)/r+\partial N_r^{(3)}/\partial r\right)+\left(M_r^{(3)}-M_\theta^{(3)}\right)/r+\partial M_r^{(3)}/\partial r-R_{rz}^{b}=(1-\mu\nabla^2)\times\left(\left(I_1^{(3)}+(h_3/2)I_0^{(3)}\right)\partial^2u_0/\partial t^2+(h_2/2)\left((h_3/2)I_0^{(3)}-I_1^{(3)}\right)\partial^2\theta_r^{(2)}/\partial t^2+\left[I_2^{(3)}-h_3I_1^{(3)}+(h_3/2)I_0^{(3)}\right]\partial^2\theta_r^{(3)}/\partial t^2\right) \quad (17d)$$

$$\delta w\colon \partial^2R_r^{(3)}/\partial r+R_r^{(3)}/r+\partial R_r^{(2)}/\partial r+R_r^{(2)}/r\ \partial^2R_r^{(1)}/\partial r+R_r^{(1)}/r=(1-\mu\nabla^2)\times\left(\left((2e_{32}V_0-N_c)\ \partial w^2/\partial r^2\right)+\left(I_0^{(1)}+I_0^{(2)}+I_0^{(3)}\right)\partial^2w_0/\partial t^2\right) \quad (17e)$$

$$\delta\varphi^{(3)}\colon \int_{-\frac{h_3}{2}}^{\frac{h_3}{2}}\left[\cos(\pi z^{(3)}/h_3)\,\partial D_r^{(3)}/\partial r+(\pi/h_3)\times\sin(\pi z^{(3)}/h_3)D_z^{(3)}\right]dz^{(3)}=0 \quad (17f)$$

$$\delta\varphi^{(3)}\colon \int_{-\frac{h_1}{2}}^{\frac{h_1}{2}}\left[\cos(\pi z^{(1)}/h_1)\,\partial D_r^{(1)}/\partial r+(\pi/h_1)\times\sin(\pi z^{(1)}/h_1)D_z^{(1)}\right]dz^{(1)}=0 \quad (17g)$$

where

$$\begin{Bmatrix}N_j^{(k)}\\M_j^{(k)}\end{Bmatrix}=\int_{-\frac{h_k}{2}}^{\frac{h_k}{2}}\sigma_j^k\begin{Bmatrix}1\\z^{(k)}\end{Bmatrix}dz^{(k)}\qquad j=r,\theta \quad (18a)$$

$$R_r^{(k)}=\int_{-\frac{h_k}{2}}^{\frac{h_k}{2}}\tau_{rz}^k\,dz^{(k)} \quad (18b)$$

$$I_f^{(k)}=\int_{-\frac{h_k}{2}}^{\frac{h_k}{2}}\rho(z)^{(k)}z^f\,dz^{(k)}\qquad f=0,1,2 \quad (18c)$$

According to Eqs. (5), (9), and (10), Eqs. (18a) and (18b) can be rewritten in the following form

$$\begin{Bmatrix}N_r^{(1)}\\M_r^{(1)}\end{Bmatrix}=\begin{Bmatrix}A_{11}^{(1)}\\B_{11}^{(1)}\end{Bmatrix}\left(\frac{\partial u_0}{\partial r}+\left(\frac{h_1}{2}\right)\frac{\partial\theta_r^{(1)}}{\partial r}+\left(\frac{h_2}{2}\right)\frac{\partial\theta_r^{(2)}}{\partial r}\right)+\frac{1}{r}\begin{Bmatrix}A_{12}^{(1)}\\B_{12}^{(1)}\end{Bmatrix}\left(u_0+\left(\frac{h_1}{2}\right)\theta_r^{(1)}+\left(\frac{h_2}{2}\right)\theta_r^{(2)}\right)+\begin{Bmatrix}B_{11}^{(1)}\\C_{11}^{(1)}\end{Bmatrix}\frac{\partial\theta_r^{(1)}}{\partial r}+\frac{1}{r}\begin{Bmatrix}B_{12}^{(1)}\\C_{12}^{(1)}\end{Bmatrix}\theta_r^{(1)} \quad (19a)$$

$$\begin{Bmatrix}N_r^{(2)}\\M_r^{(2)}\end{Bmatrix}=\begin{Bmatrix}A_{11}^{(2)}\\B_{11}^{(2)}\end{Bmatrix}\frac{\partial u_0}{\partial r}+\frac{1}{r}\begin{Bmatrix}A_{12}^{(2)}\\B_{12}^{(2)}\end{Bmatrix}u_0+\begin{Bmatrix}B_{11}^{(2)}\\C_{11}^{(2)}\end{Bmatrix}\frac{\partial\theta_r^{(2)}}{\partial r}+\frac{1}{r}\begin{Bmatrix}B_{12}^{(2)}\\C_{12}^{(2)}\end{Bmatrix}\theta_r^{(2)} \quad (19b)$$

$$\begin{Bmatrix}N_r^{(3)}\\M_r^{(3)}\end{Bmatrix}=\begin{Bmatrix}A_{11}^{(3)}\\B_{11}^{(3)}\end{Bmatrix}\left(\frac{\partial u_0}{\partial r}-\left(\frac{h_3}{2}\right)\frac{\partial\theta_r^{(3)}}{\partial r}-\left(\frac{h_2}{2}\right)\frac{\partial\theta_r^{(2)}}{\partial r}\right)+\frac{1}{r}\begin{Bmatrix}A_{12}^{(3)}\\B_{12}^{(3)}\end{Bmatrix}\left(u_0-\left(\frac{h_3}{2}\right)\theta_r^{(3)}-\left(\frac{h_2}{2}\right)\theta_r^{(2)}\right)+\begin{Bmatrix}B_{11}^{(3)}\\C_{11}^{(3)}\end{Bmatrix}\frac{\partial\theta_r^{(3)}}{\partial r}+\frac{1}{r}\begin{Bmatrix}B_{12}^{(3)}\\C_{12}^{(3)}\end{Bmatrix}\theta_r^{(3)} \quad (19c)$$

$$\begin{Bmatrix}N_\theta^{(1)}\\M_\theta^{(1)}\end{Bmatrix}=\begin{Bmatrix}A_{12}^{(1)}\\B_{12}^{(1)}\end{Bmatrix}\left(\frac{\partial u_0}{\partial r}+\left(\frac{h_1}{2}\right)\frac{\partial\theta_r^{(1)}}{\partial r}+\left(\frac{h_2}{2}\right)\frac{\partial\theta_r^{(2)}}{\partial r}\right)+\frac{1}{r}\begin{Bmatrix}A_{22}^{(1)}\\B_{22}^{(1)}\end{Bmatrix}\left(u_0+(\frac{h_1}{2})\theta_r^{(1)}+(\frac{h_2}{2})\theta_r^{(2)}\right)+\begin{Bmatrix}B_{12}^{(1)}\\C_{12}^{(1)}\end{Bmatrix}\frac{\partial\theta_r^{(1)}}{\partial r}+\frac{1}{r}\begin{Bmatrix}B_{22}^{(1)}\\C_{22}^{(1)}\end{Bmatrix}\theta_r^{(1)} \quad (19d)$$

$$\begin{Bmatrix}N_\theta^{(2)}\\M_\theta^{(2)}\end{Bmatrix}=\begin{Bmatrix}A_{12}^{(2)}\\B_{12}^{(2)}\end{Bmatrix}\frac{\partial u_0}{\partial r}+\frac{1}{r}\begin{Bmatrix}A_{22}^{(2)}\\B_{22}^{(2)}\end{Bmatrix}u_0+\begin{Bmatrix}B_{12}^{(2)}\\C_{12}^{(2)}\end{Bmatrix}\frac{\partial\theta_r^{(2)}}{\partial r}+\frac{1}{r}\begin{Bmatrix}B_{22}^{(2)}\\C_{22}^{(2)}\end{Bmatrix}\theta_r^{(2)} \quad (19e)$$

$$\begin{Bmatrix}N_\theta^{(3)}\\M_\theta^{(3)}\end{Bmatrix}=\begin{Bmatrix}A_{12}^{(3)}\\B_{12}^{(3)}\end{Bmatrix}\left(\frac{\partial u_0}{\partial r}-\left(\frac{h_3}{2}\right)\frac{\partial\theta_r^{(3)}}{\partial r}-\left(\frac{h_2}{2}\right)\frac{\partial\theta_r^{(2)}}{\partial r}\right)+\frac{1}{r}\begin{Bmatrix}A_{22}^{(3)}\\B_{22}^{(3)}\end{Bmatrix}\left(u_0-(\frac{h_3}{2})\theta_r^{(3)}-(\frac{h_2}{2})\theta_r^{(2)}\right)+\begin{Bmatrix}B_{12}^{(3)}\\C_{12}^{(3)}\end{Bmatrix}\frac{\partial\theta_r^{(3)}}{\partial r}+\frac{1}{r}\begin{Bmatrix}B_{22}^{(3)}\\C_{22}^{(3)}\end{Bmatrix}\theta_r^{(3)} \quad (19f)$$

$$R_r^{(1)}=A_{44}^{(1)}\left(\theta_r^{(1)}+\frac{\partial w}{\partial r}\right) \quad (19g)$$

$$R_r^{(2)}=A_{44}^{(2)}\left(\theta_r^{(2)}+\frac{\partial w}{\partial r}\right) \quad (19h)$$

$$R_r^{(3)}=A_{44}^{(3)}\left(\theta_r^{(3)}+\frac{\partial w}{\partial r}\right) \quad (19i)$$

in which

$$\begin{Bmatrix} A_{nm}^{(k)} \\ B_{nm}^{(k)} \\ C_{nm}^{(k)} \end{Bmatrix} = \int_{-\frac{h_k}{2}}^{\frac{h_k}{2}} Q_{nm}^{k} \begin{Bmatrix} 1 \\ z^{(k)} \\ z^{(k)^2} \end{Bmatrix} dz^{(k)} \qquad n,m = 1,2,4 \quad (20)$$

4. The mathematical forms of the edge conditions

In the present paper, the general boundary conditions are utilized. Using in-plane and transverse restraining springs, the general boundary conditions for the inner and outer edges of the FG-CNTRC piezoelectric sandwich annular nanoplates can be written as follows (Alipour 2016):

• General boundary conditions at the inner edge

$$\begin{aligned} &\left(N_r^{(1)} + N_r^{(2)} + N_r^{(3)} - (h_1 + h_2 + h_3)k_u^i u_0 - \right. \\ &(h_1^2/2)k_u^i \theta_r^{(1)} - (h_2/2)(h_1 - h_3)k_u^i \theta_r^{(2)} + \\ &\left.(h_3^2/2)k_u^i \theta_r^{(3)}\right) = 0 \end{aligned} \quad (21a)$$

$$\begin{aligned} &\left((h_1/2)N_r^{(1)} + M_r^{(1)} - (h_1^3/12)k_u^i \theta_r^{(1)} - (h_1^2/2)k_u^i \right. \\ &\left.\left(u_0 + (h_1/2)\theta_r^{(1)} + (h_1/2)\theta_r^{(2)}\right)\right) = 0 \end{aligned} \quad (21b)$$

$$\begin{aligned} &\left((h_2/2)N_r^{(1)} + M_r^{(1)} - (h_2/2)N_r^{(1)} - (h_2/2)(h_1 - h_3)\right. \\ &k_u^i u_0 - (h_2/2)(h_1^2/2)k_u^i \theta_r^{(1)} - (h_2^2/4)(h_1 + h_3 + h_2/3) \\ &\left.k_u^i \theta_r^{(2)} - (h_3^2/2)(h_2/2)k_u^i \theta_r^{(3)}\right) = 0 \end{aligned} \quad (21c)$$

$$\begin{aligned} &\left((-h_3/2)N_r^{(3)} + M_r^{(3)} - (h_3^3/12)k_u^i \theta_r^{(3)} + (-h_3^2/2)\right. \\ &\left.k_u^i\left(u_0 + (h_3/2)\theta_r^{(3)} + (h_2/2)\theta_r^{(2)}\right)\right) = 0 \end{aligned} \quad (21d)$$

$$\left(R_r^{(1)} + R_r^{(2)} + R_r^{(3)} - k_w^i w\right) = 0 \quad (21e)$$

• General boundary conditions at the outer edge

$$\begin{aligned} &\left(N_r^{(1)} + N_r^{(2)} + N_r^{(3)} - (h_1 + h_2 + h_3)k_u^o u_0 - (h_1^2/2)\right. \\ &\left.k_u^o \theta_r^{(1)} - (h_2/2)(h_1 - h_3)k_u^o \theta_r^{(2)} + (h_3^2/2)k_u^o \theta_r^{(3)}\right) = 0 \end{aligned} \quad (22a)$$

$$\begin{aligned} &\left((h_1/2)N_r^{(1)} + M_r^{(1)} - (h_1^3/12)k_u^o \theta_r^{(1)} - (h_1^2/2)k_u^o \times \right. \\ &\left.\left(u_0 + (h_1/2)\theta_r^{(1)} + (h_2/2)\theta_r^{(2)}\right)\right) = 0 \end{aligned} \quad (22b)$$

$$\begin{aligned} &\left((h_2/2)N_r^{(1)} + M_r^{(1)} - (h_2/2)N_r^{(1)} - (h_2/2)(h_1 - h_3)\right. \\ &k_u^o u_0 - (h_2/2)(h_1^2/2)k_u^o \theta_r^{(1)} - (h_2^2/4)(h_1 + h_3 + h_2/3) \\ &\left.k_u^o \theta_r^{(2)} - (h_3^2/4)(h_2/2)k_u^o \theta_r^{(3)}\right) = 0 \end{aligned} \quad (22c)$$

$$\begin{aligned} &\left((-h_3/2)N_r^{(3)} + M_r^{(3)} - (h_3^3/12)k_u^o \theta_r^{(3)} + (-h_3/2)k_u^o\right) \\ &\times \left(u_0 + (h_3/2)\theta_r^{(3)} + (h_2/2)\theta_r^{(2)}\right) = 0 \end{aligned} \quad (22d)$$

$$\left(R_r^{(1)} + R_r^{(2)} + R_r^{(3)} - k_w^o w\right) = 0 \quad (22e)$$

According to the presented approach, the classical boundary conditions at the inner and outer edges may be simulated by setting the stiffness parameters of elastic edges as follows:

• At the inner edge:

$$\begin{cases} \text{Clamped edge: } k_u^i, k_w^i \to \infty \quad (k_u^i = k_w^i = 10^{20}) \\ \text{Simply supported: } k_u^i = 0, k_w^i \to \infty \quad (k_w^i = 10^{20}) \\ \text{Free edge: } k_u^i = k_w^i = 0 \end{cases}$$

• At the outer edge:

$$\begin{cases} \text{Clamped edge: } k_u^o, k_w^o \to \infty \quad (k_u^o = k_w^o = 10^{20}) \\ \text{Simply supported: } k_u^o = 0, k_w^o \to \infty \quad (k_w^o = 10^{20}) \\ \text{Free edge: } k_u^o = k_w^o = 0 \end{cases}$$

5. DQM to solve the motion equation

Among numerical solution procedures, DQM is selected because it needs less grid points to present accurate answer and satisfies various boundary conditions. In this procedure, differential equations are varied into a first-order algebraic equation by applying suitable weighting coefficients, since weighting coefficients do not appertain to any special topic and only relate to the grid spacing. Actually, the partial derivatives of a function ($f(r)$) are estimated according to a specific variable (r) at a discontinuous point in a domain defined as a set of linear weighting coefficients. The approximation of the derivative function with respect to r may be written in the general form as (Bellman and Casti 1971)

$$\frac{\partial^n F(r_j)}{\partial r^n} = \sum_{k=1}^{N} A_{jk}^{(n)} F(r_k) \qquad n = 1, \ldots N-1 \quad (23)$$

where N denotes the number of points in r direction and $A_{jk}^{(n)}$ shows the weighting coefficients. The Chebyshev-Gauss-Lobatto polynomial is utilized to determine the spaced place of the grid points as (Talebitooti 2013)

$$r_j = r_i + \frac{r_o - r_i}{2}\left(1 - cos\left(\frac{2j-1}{N-1}\right)\pi\right) \quad (24)$$

where r_i and r_o are the inner radius and outer radius, respectively.

5.1 Free vibration response

In order to obtain existing natural frequency of nano structure, the applied compressive load, N_c, should be disregarded in Eq. (17). For obtaining the eigenvalue related to equations, degrees of freedom can be divided into domain as well as boundary degrees of freedom as follow

$$\{Y\}_d = \begin{Bmatrix} u_0 \\ \theta_r^{(1)} \\ \theta_r^{(2)} \\ \theta_r^{(3)} \\ w \\ \phi^{(1)} \\ \phi^{(3)} \end{Bmatrix}_d, \quad \{Y\}_b = \begin{Bmatrix} u_0 \\ \theta_r^{(1)} \\ \theta_r^{(2)} \\ \theta_r^{(3)} \\ w \\ \phi^{(1)} \\ \phi^{(3)} \end{Bmatrix}_b \quad (25)$$

in which subscripts b and d respectively describe boundary

Table 1 Material properties of polymeric matrix, SWCNT, ZnO, PZT4 and PZT-5A

Property	CNTs, PPP	PZT4	PZT-5A	ZnO
Young's modulus (GPa)	$E_{11}^{cnt} = 5646.6$ $E_{22}^{cnt} = 7080$ $E_{12}^{cnt} = 1944.5$ $E^{m} = 8.3$	$Q_{11} = 132$ $Q_{12} = 71$ $Q_{33} = 115$ $Q_{13} = 73$ $Q_{44} = 26$	$Q_{11} = 121$ $Q_{12} = 75.9$ $Q_{33} = 111$ $Q_{13} = 75.4$ $Q_{44} = 21.1$	$Q_{11} = 207$ $Q_{12} = 117.7$ $Q_{33} = 209.5$ $Q_{13} = 106$ $Q_{44} = 44.8$
Poisson ratio	$\upsilon^{cnt} = 0.175$ $\upsilon^{m} = 0.18$	-	-	-
Mass density (kg/m^3)	$\rho^{cnt} = 4000$ $\rho^{m} = 1750$	7500	7750	6316
e_{31} (C/m^2)	-	-4.1	-5.4	-0.51
e_{33} (C/m^2)	-	14.1	15.8	1.22
e_{15} (C/m^2)	-	10.5	12.3	-0.45
$\in_{11}$ (nF/m)	-	7.124	8.11	7.77
$\in_{33}$ (nF/m)	-	5.841	7.35	8.91

and domain degrees of freedom. With arranging the separated equations of motions again, the assembled formation related to these equations into a matrix form can be written as below

$$[K_{dd}]\{Y\}_d + [K_{db}]\{Y\}_b - \omega^2[M]\{Y\}_d = \{0\} \quad (26a)$$

in which $[K]$ is the stiffness matrix and $[M]$ is the mass matrix, respectively; and ω is the frequency. In a same state, the separated form of boundary edges can become

$$[K_{bb}]\{Y\}_b + [K_{bd}]\{Y\}_b = \{0\} \quad (26b)$$

In the relations mentioned above, the stiffness matrix's components including K_{dd}, K_{db}, K_{bd} and K_{bb} can be achieved simply according to description of vectors relative to boundary as well as domain degrees of freedom from the correlated equations. Removing $\{Y\}_b$ from Eq. (26a) yields

$$[K]\{Y\}_d - \omega^2[M]\{Y\}_d = \{0\} \quad (26c)$$

in which

$$[K] = [K_{dd}] - [K_{db}][K_{bb}]^{-1}[K_{bd}] \quad (26d)$$

Finally, solution of above equations, the natural frequencies of this structure are achieved.

5.2 Bucking response

In this section, buckling load of an embedded sandwich annular nanoplate subjected to uniform compressive load is obtained. Similarly, the buckling response of the sandwich nano structure can be attained using DQM by disregarding time harmonic factors in Eq. (17). Hence, in order to obtain the critical buckling loads the following equations can be solved.

Table 2 The first three dimensionless frequencies for FG-CNTRC sandwich annular plate

Boundary conditions	V_{cnt}^*	Dimensionless frequencies		
		$\bar{\omega}_1$	$\bar{\omega}_2$	$\bar{\omega}_3$
C-C	0.11	5.9170	11.3925	16.0653
	0.14	5.9817	11.5169	16.2294
S-C	0.11	5.1613	10.4908	15.2573
	0.14	5.2163	10.6100	15.4209
C-S	0.11	4.2464	8.3935	12.9514
	0.14	4.2699	8.4550	13.0723
S-S	0.11	3.5316	7.6687	12.5729
	0.14	3.5480	7.7375	12.7024

$$[K_{dd} + N_c]\{Y\}_d + [K_{db}]\{Y\}_b = \{0\} \quad (27)$$

It should be noticed that for applying the DQM to the equations of motion and boundary edges in order to obtain critical buckling loads the mentioned Eqs. (26a)-(26d) are utilized as well.

6. Numerical results and discussion

The buckling and vibration analysis of the FG-CNTRC sandwich annular nanoplates bounded with piezoelectric layers with edges elastically restrained under electric field is studied in this paper. In this section, the effects of some main parameters such as the value of spring coefficients, small-scale effect, external voltage, volume fractions, distributions of CNTs, thickness, and radius ratios on the buckling louds and vibration are analyzed. The effective material properties of PPP matrix, SWCNT, and different substances as piezoelectric layers are presented in Table 1 (Hosseini Hashemi *et al*. 2010).

Table 3 Comparison of first three frequencies (Hz) of sandwich annular plate

Boundary edges	Power index g	Frequency	Method			
			CPT (Ebrahimi and Rastgoo 2008)	FSDT (Ebrahimi *et al*. 2009)	TSDT (Hosseini Hashemi *et al*. 2010)	Present work
C-C	1	ω_1	435.87	428.6	430.723	431.21
		ω_2	1205.8	1163.35	1170.51	1171.63
	3	ω_1	429.58	422.63	425.478	426.85
		ω_2	1187.34	1147.84	1156.37	1158.31
C-S	1	ω_1	287.48	284.83	283.511	282.22
		ω_2	966.92	945.27	943.950	941.53
	3	ω_1	284.17	281.48	280.053	279.76
		ω_2	955.63	934.15	932.514	930.63
S-C	1	ω_1	344.29	341.06	341.118	342.19
		ω_2	1028.87	1004.26	1004.34	1005.71
	3	ω_1	340.41	336.77	336.956	337.95
		ω_2	1016.86	991.24	992.165	993.16
S-S	1	ω_1	216.6	215.13	215.791	215.94
		ω_2	811.05	793.69	795.570	794.86
	3	ω_1	214.67	212.84	213.155	213.06
		ω_2	800.68	783.53	785.903	785.62

Table 4 Comparison of non-dimensional critical buckling load

r_i/r_o	Reference	h/r_o				
		0.01	0.05	0.1	0.2	0.3
0.1	Malekzadeh and Ouji (2008)	3.9840	3.9696	3.9303	3.7813	3.5598
	Present	3.9531	3.9342	3.9110	3.7687	3.5401
0.3	Malekzadeh and Ouji (2008)	3.1067	3.0978	3.0726	2.9761	2.8299
	Present	2.9854	2.9776	2.9702	2.9421	2.9156
0.5	Malekzadeh and Ouji (2008)	2.5001	2.4951	2.4776	2.4097	2.3053
	Present	2.4820	2.4642	2.4463	2.3867	2.2861

The CNT efficiency factors presented in Eqs. (5a)-(5c) are approximated through matching Young's Modulus (E_{11} and E_{22}) related to CNTRCs estimated from ROM (Guo *et al*. 2019). For instance,$\eta_1 = 0.149$, $\eta_2 = \eta_3 = 0.934$ for $V_{cnt}^* = 0.11$, $\eta_1 = 0.150$, $\eta_2 = \eta_3 = 0.941$ for $V_{cnt}^* = 0.14$ and $\eta_1 = 0.149$, $\eta_2 = \eta_3 = 1.381$ for $V_{cnt}^* = 0.17$. For convenience, the following non-dimensional frequency is utilized in proposing the numerical results in the graphical and tabular form

$$\bar{\omega} = \omega r_i^2 \sqrt{\frac{\rho_1 \hbar_1}{D\pi^4}} \tag{28}$$

in which

$$D = E_m h_1^3 / 12(1 - \upsilon_m^2) \tag{29}$$

Meanwhile, the influences of different volume fractions and various classical edge conditions of FG-CNTRC piezoelectric sandwich annular nanoplates on the first three dimensionless frequencies are given in Table 2. For the mentioned table, the small scale effect is $e_0 a = 1$ (nm) and the CNTRC annular nanoplates is assumed in UD type.

So far, no study has investigated the vibration of FG-CNTRC annular nanoplates covered by piezoelectric layers with edges elastically restrained against in-plane and transverse displacements based on the LW theory using DQM and nonlocal piezoelectricity theory. Therefore, the validation of the paper is not possible. Still, in order to verify this research as far as possible, a simplified analysis of this paper is performed without considering edges elastically restrained against in-plane and transverse displacements, small-scale effect, and FG-CNTRC. For vibration validation, results are compared with the study by Hosseini Hashemi *et al*. (2010) who performed the closed-form vibration analysis of thick annular FG plates with integrated piezoelectric layers. In Table 3, the first three frequencies based on classical plate theory (CPT), FSDT, and third order shear deformation theory (TSDT) are presented. the first three frequencies written for C-C, C-S, S-C and S-S boundary conditions in this Table. The thickness-radius ratio is $\frac{h}{r_o} = \frac{1}{20}$, in which h indicates the height of the core layer and the selected piezoelectric substance is PZT4. It is evident that the LW theory ensures correct results if compared with references (Ebrahimi and Rastgoo 2008, Ebrahimi *et al*. 2009, Hosseini Hashemi *et al*. 2010).

As seen, the obtained result of present work in a good agreement with other results obtained, in particular, with TSDT which proves the LW theory precision. As

Table 5 Influence of different volume fractions on the dimensionless critical buckling load

e_0a (nm)	V^*_{cnt}	Thickness ratio, h_2/h_1				
		2.0	2.5	3.0	3.5	4.0
0.0	0.11	31.494	41.959	53.823	66.999	81.397
	0.14	32.130	43.065	55.539	69.459	84.721
	0.17	32.778	44.192	57.286	71.959	88.094
0.5	0.11	24.887	33.170	42.537	52.885	64.092
	0.14	25.392	34.049	43.900	54.828	66.689
	0.17	25.907	34.946	45.289	56.807	69.334
1.0	0.11	14.333	18.079	21.844	25.678	29.572
	0.14	14.637	18.559	22.500	26.511	30.579
	0.17	14.953	19.060	23.190	27.388	31.642

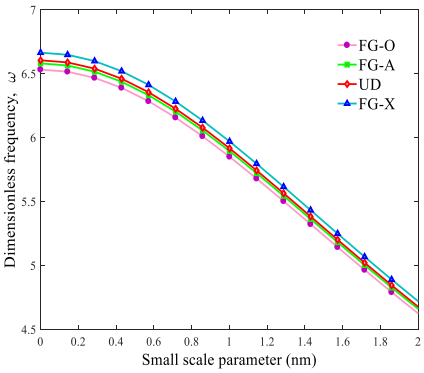

(a) Different type of CNTs distribution

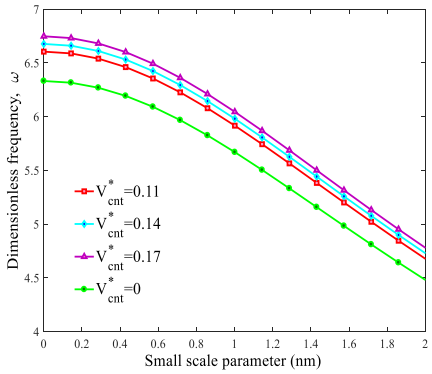

(b) Volume fraction of CNTs

Fig. 2 Dimensionless frequency versus small scale parameter

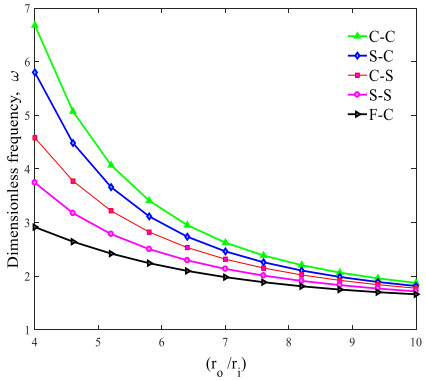

Fig. 3 Dimensionless frequency versus the radius ratio for different boundary conditions: C-C, S-C, C-S, S-S, F-C

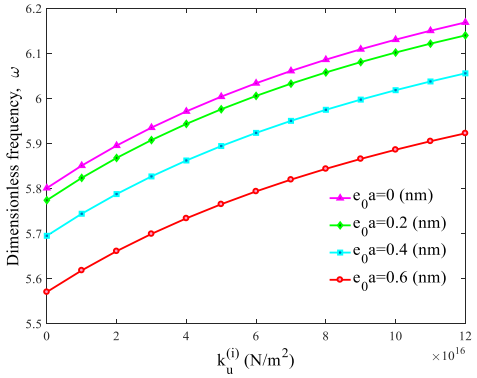

(a) Inner in-plane (k_u^i) spring coefficient

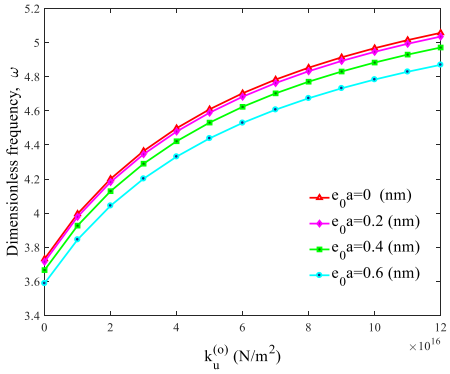

(b) Outer in-plane (k_u^o) spring coefficient

Fig. 4 Effects of the small scale on the dimensionless frequency of structure

mentioned, there is no work looking into buckling analysis of FG-CNTRC annular nanoplate integrated by piezo-electric layers and enclosed by inner and outer edges elastically restrained using LW and DQM. Validation of this structure would be impossible unless some simplification so as to match it up to other structures analyzed in other paper. In one work carried out by Malekzadeh and Ouji (2008), buckling analysis of annular plate based on DQM which is put under an external pressure at the end of surface, has been investigated. In Table 4, the data derived from present work have been compared by Malekzadeh and Ouji (2008) in which the supposed boundary condition is free-simply supported. The results are primed for various values of thickness and radius ratios. In this section the non-dimensional parameter can be written as

$$P_{cr} = Ph\frac{r_o^2}{D} \tag{30}$$

Similarly, the far-reaching effects of different volume fractions on the dimensionless critical buckling load of FG-CNTRC piezoelectric sandwich annular nanoplates are exhibited in Table 5. Depicted in that table, these

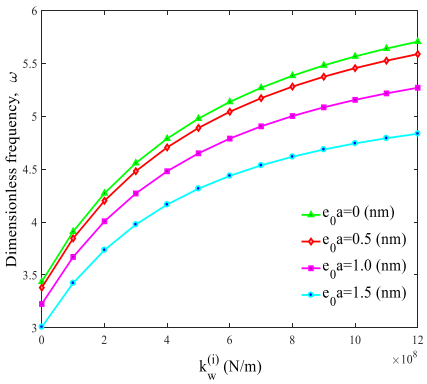

(a) Inner transverse (k_w^i) spring coefficient

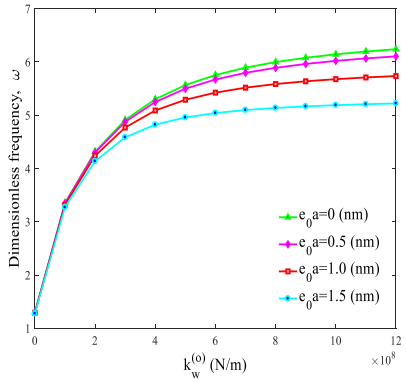

(b) Outer transverse (k_w^o) spring coefficient

Fig. 5 Effects of the small scale on the dimensionless frequency of structure

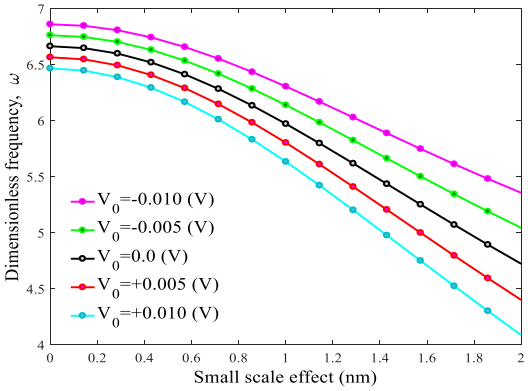

Fig. 6 Dimensionless frequency versus small scale parameter for various external applied voltage

dimensionless critical loads are attained by considering C-C boundary condition, UD distribution and the regarded non-dimensional term can be defined as

$$N^* = N_c r_i^2 / Q_{11}^c h_1^3 \tag{31}$$

6.1 Free vibration analysis

The efficacy and advantage of using CNTs as reinforcements are shown in Figs. 2(a)-(b). Fig. 2(a) illustrates the effect of various types of FG distributions of CNTs on the frequency of structure versus small-scale

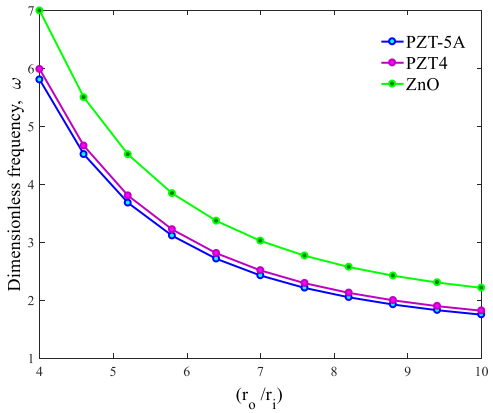

Fig. 7 Dimensionless frequency versus the radius ratio for different piezoelectric layers

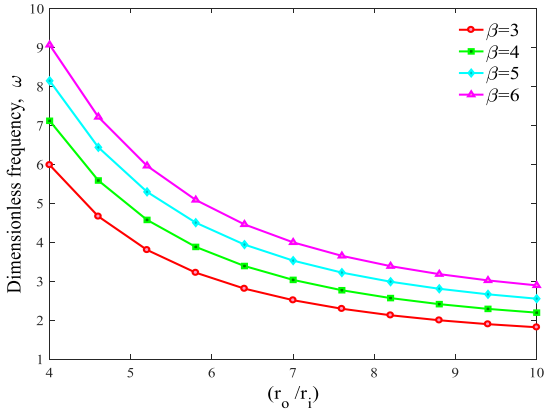

Fig. 8 Dimensionless frequency versus the radius ratio for various thickness ratio

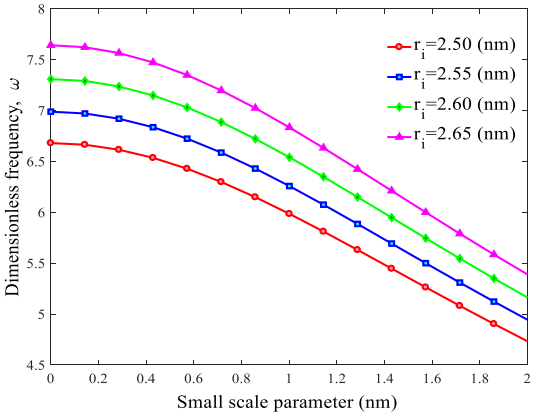

Fig. 9 Dimensionless frequency versus small scale parameter for different inner radius of annular nanoplates

parameter. It is obvious that the $FG-O$ distribution of CNTs has the least effect on frequency. Instead, the $FG-X$ distribution brings out a higher frequency because the aggregation of CNTs is close to the top and bottom of the layer. It is obvious that the results of UD and $FG-A$ types are close. Also, the influence of volume fractions of

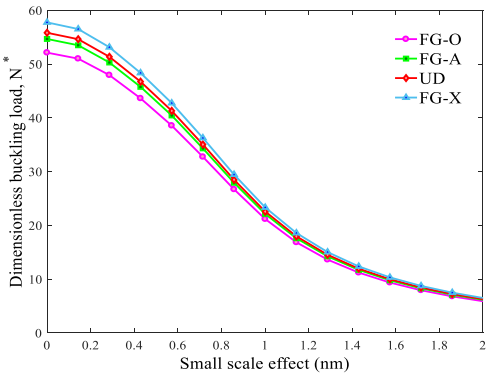

Fig. 10 Dimensionless buckling load versus small scale parameter for different type of CNTs distribution

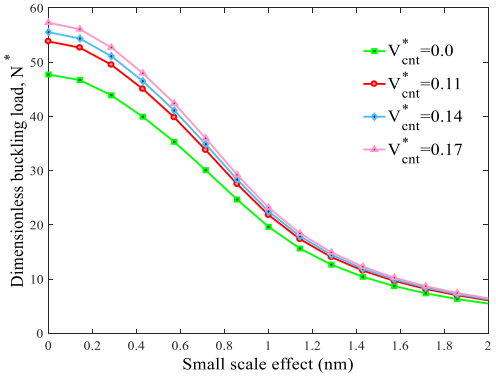

Fig. 11 Dimensionless buckling load versus small scale parameter for various volume fraction of CNTs

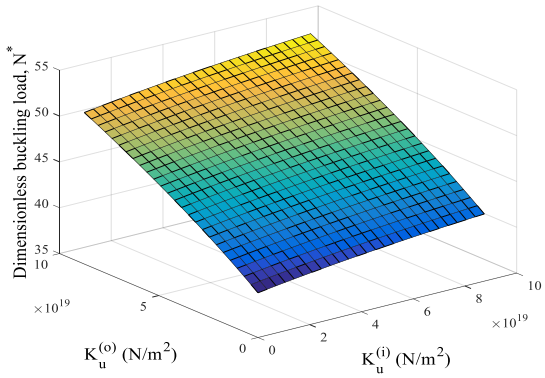

(a) Inner (k_u^i) and outer (k_u^o) in-plane spring coefficient

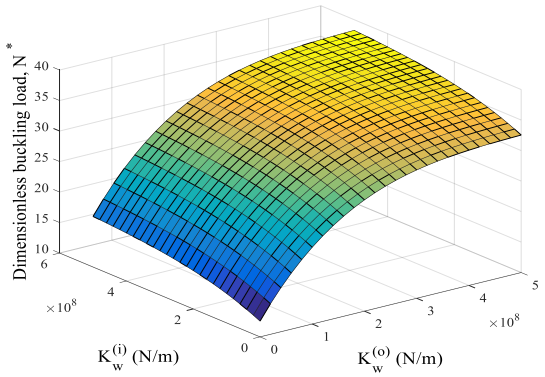

(b) Inner (k_w^i) and outer (k_w^o) in-plane spring coefficient

Fig. 12 Effects of the small scale on the dimensionless frequency of structure

CNTs on the amount and magnitude of the sandwich annular nanoplates frequency is depicted in Fig. 2(b). With increasing the volume fraction of CNTs, frequency increases. It can be justified by this reason that stiffness of the structure rises. The boundary conditions at both edges of the structure are supposed as C-C and the thickness ratio is $\frac{h_2}{h_1} = 3$.

Fig. 3. display the influences of different classical boundary conditions on the dimensionless frequency with respect to the radius ratio. It is clear that C-C is the strongest type of boundary conditions and F-C is the least strong one. The C-C type of boundary conditions makes the system stiffer. Based on this figure, it can be understood that the assuming clamped support at the outer edge is more effective than the one at the inner edge and makes the system more stable. It must be noted that by enhancing the radius ratio, the dimensionless frequency decreases. The amount of small-scale parameter and volume fractions of CNTs is assumed $e_0 a = 0\ (nm)$ and $V_{cnt}^* = 0.14$, respectively.

The effects of the small scales on the dimensionless frequency of the FG-CNTRC piezoelectric sandwich annular nanoplates with respect to inner in-plane (k_u^i) and outer in-plane (k_u^o) spring coefficients are illustrated in Figs. 4(a)-(b), respectively, where the other coefficients have infinite values. It is clear that the increment of in-plane resistances of edges leads to an increase in the dimensionless frequency because the stiffness of the structure increases. Fig. 4(b) shows that the effect of outer in-plane spring coefficients on the dimensionless frequency is much more in comparison to the inner in-plane spring coefficient.

Figs. 5(a)-(b) illustrate the variations of the dimensionless frequency of the nanostructure as a function of inner transverse (k_w^i) and outer transverse (k_w^o) spring coefficients by varying the small-scale effect parameter where the other coefficients have infinite values as well. Based on Fig. 5(a), it is concluded that the effect of inner transverse spring stiffness is less than that of the outer transverse spring stiffness. Also, the dimensionless frequency increases with increasing the transverse spring.

The dimensionless frequency according to different amounts of external applied voltages versus the small-scale parameter is plotted in Fig. 6. As can be seen, the dimensionless frequency decreases by applying external voltages from negative to positive values. Indeed, imposing negative and positive external voltages causes tensile and axial compressive forces on the bottom and top of the face sheet layer. Therefore, the applied external voltage is an effective controlling case for the frequency of the system.

Fig. 7 illustrates the efficacy of various piezoelectric layers as face sheets and their effects on the frequency and mechanical behavior of the sandwich annular nanoplates versus the radius ratio. Based on this figure, it can be inferred that the use of ZnO makes the system stiffer, and

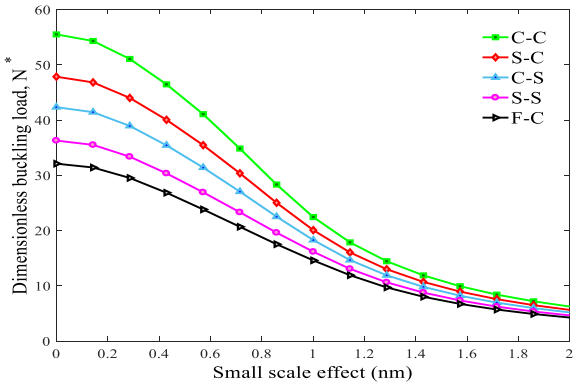

Fig. 13 Dimensionless buckling load versus the radius ratio for different boundary conditions: C-C, S-C, C-S, S-S, F-C

the dimensionless frequency is therefore increased. PZT-5A has the lowest effect on the dimensionless frequency of the structure from among these three substances. This figure satisfies the use of ZnO beside its other advantages.

The effect of thickness ratio $(\beta = \frac{h_2}{h_1})$ on dimensionless frequency in terms of radius ratio is evident in Fig. 8. In this figure, the volume fraction and small-scale effect are assumed to be $V_{cnt}^{*} = 0.14$ and $e_0 a = 1\ (nm)$ respectively. It is concluded that the dimensionless frequency increases with increasing the thickness ratio. This is because the higher amount of thickness ratio makes the system stiffer and more stable.

Finally, Fig. 9 indicates the influence of the inner radius of the FG-CNTRC piezoelectric sandwich annular nano-plates on the dimensionless frequency with respect to the dimensionless nonlocal parameter. With the increment of the inner radius, dimensionless frequency increases. It is evident that the dimensionless frequency increases with the increment of inner radius due to increasing the system stiffness. Hence, for the optimum design of nanostructures, a low inner radius is one of the best options. In this figure, $V_{cnt}^{*} = 0.14$ is considered for the volume fraction of CNTs and the C-C type of boundary conditions is assumed.

6.2 Buckling analysis

Fig. 10 depicts the influence of different types of FG distribution of CNTs on the critical buckling load, versus small scale effect. As expected, the $FG - X$ distribution of CNTs results higher critical buckling loads. This is due to the fact that in this stance, SWCNTs are close to the top and bottom of the core layer. Hence, the stiffness of the whole structure mounts up. It should be noticed, the results of UD and $FG - A$ types are close to each other and $FG - O$ distribution has the least influence on the critical buckling load. Moreover, the hypothesized values of volume fraction, radial and thickness ratios are regarded respectively $V_{cnt}^{*} = 0.14$, $\frac{r_o}{r_i} = 4$ and $\beta = 3$.

Changes in critical buckling load due to different CNTs volume fraction versus small scale effect, are shown in Fig. 11. It is apparent from Fig. 11, rise in CNTs volume fraction bring about increase in critical buckling loads. That arises because increasing the volume fraction of CNTs can augment the stiffness of the structure. Supposed voltage, thickness ratio and radial ratio in this figure are respectively $V_0 = 0$, $\beta = 3$ and $\frac{r_o}{r_i} = 4$.

In order to discover how the inner and outer transverse spring coefficients, (k_w^i) and (k_w^o), as well as, inner and outer in-plane spring coefficients, (k_u^i) and (k_u^o), affect the critical buckling load, the different values of these coefficients and its effect on the dimensionless buckling load are investigated. Figs. 12(a)-(b) manifest three dimensional plot of dimensionless buckling load versus inner and outer (in-plane and transverse) spring coefficients. It is obvious that increasing spring coefficients lead to increasing the dimensionless buckling load. As observed, the effects of inner and outer transverse spring coefficients can be regarded as more efficient parameter in comparison with in-plane spring coefficients.

The influences of different classical boundary conditions on the dimensionless critical buckling load with respect to the small scale effect are shown in Fig. 13. As observed, using clamped support make the system stiffer and more stable, so the annular sandwich plate can bear larger loads than simply supported and free edge. Given this figure, it can be understood the assuming clamped support at the inner edge is less effective than the one at the outer edge and makes the system less stable. The values of and volume fractions of CNTs, radial and thickness ratios are hypothesized $V_{cnt}^{*} = 0.14$, $\beta = 3$ and $\frac{r_o}{r_i} = 4$, respectively.

7. Conclusions

For the first time, a size-dependent vibration and buckling analysis of an FG-CNTRC annular nanoplates with integrated piezoelectric layers under various elastically restrained edges was performed in this article. The sandwich structure was subjected to an electric field. To obtain accurate results, the LW theory and nonlocal piezoelectricity were taken into account. Hamilton's principle and the energy method were engaged to derive governing motion equations. The governing equations were solved using DQM. Comparisons revealed that the results based on the presented method for the FG-CNTRC piezoelectric sandwich annular nanoplates with classical edge conditions as some special types of elastic supports are highly in agreement with the results of the CPT and FSDT. Also, exhaustive analyses were conducted to evaluate the effect of various stiffness parameters of in-plane and transverse elastic restraints. In particular, the negative and positive external voltages cause tensile and axial compressive forces. It is concluded that the increase in voltage values causes a decrease in the dimensionless both critical buckling load and frequency of the system. $FG - X$ and $FG - O$ distributions of CNTs in the structure had the maximum and minimum stiffness, respectively. It is expected that the results would be helpful for the study and design of NEMS and MEMS.

References

Alipour, M. (2016), "Effects of elastically restrained edges on FG sandwich annular plates by using a novel solution procedure based on layerwise formulation", *Arch. Civ. Mech. Eng.*, **16**(4), 678-694. https://doi.org/10.1016/j.acme.2016.04.015.

Alipour, M. and Shariyat, M. (2017), "Analytical layerwise free vibration analysis of circular/annular composite sandwich plates with auxetic cores", *Int. J. Mech. Mater. Des.*, **13**(1), 125-157. https://doi.org/10.1007/s10999-015-9321-2.

Ansari, R., Torabi, J. and Shojaei, M.F. (2017), "Buckling and vibration analysis of embedded functionally graded carbon nanotube-reinforced composite annular sector plates under thermal loading", *Compos. Part B Eng.*, **109**, 197-213. https://doi.org/10.1016/j.compositesb.2016.10.050.

Bellman, R. and Casti, J. (1971), "Differential quadrature and long-term integration", *J. Math. Anal. Appl.*, **34**(2), 235-238. https://doi.org/10.1016/0022-247X(71)90110-7.

Burman, M. and Zenkert, D. (2000), "Fatigue of undamaged and damaged honeycomb sandwich beams", *J. Sandw. Struct. Mater.*, **2**(1), 50-74. https://doi.org/10.1177/109963620000200103.

Ebrahimi, F. and Rastgoo, A. (2008), "Free vibration analysis of smart annular FGM plates integrated with piezoelectric layers", *Smart Mater. Struct.*, **17**(1), 015044. https://doi.org/10.1088/0964-1726/17/1/015044.

Ebrahimi, F. and Habibi, S. (2017), "Low-velocity impact response of laminated FG-CNT reinforced composite plates in thermal environment", *Adv. Nano Res., Int. J.*, **5**(2), 69-97. https://doi.org/10.12989/anr.2017.5.2.069.

Ebrahimi, F., Rastgoo, A. and Atai, A. (2009), "A theoretical analysis of smart moderately thick shear deformable annular functionally graded plate", *Eur. J. Mech. A Solids*, **28**(5), 962-973. https://doi.org/10.1016/j.euromechsol.2008.12.008.

Ebrahimi, F., Karimiasl, M., Civalek, O. and Vinyas, M. (2019), "Surface effects on scale-dependente vibration behavior of flexoelectric sandwich nanobeams", *Adv. Nano Res., Int. J.*, **7**(9), 77-88. http://dx.doi.org/10.12989/anr.2019.7.2.077.

Eringen, A.C. (1983), "On differential equations of nonlocal elasticity and solutions of screw dislocation and surface waves", *J. Appl. Phys.*, **54**(9), 4703-4710. https://doi.org/10.1063/1.332803.

Ferreira, A., Fasshauer, G., Batra, R. and Rodrigues, J. (2008), "Static deformations and vibration analysis of composite and sandwich plates using a layerwise theory and RBF-PS discretizations with optimal shape parameter", *Compos. Struct.*, **86**(4), 328-343. https://doi.org/10.1016/j.compstruct.2008.07.025.

Gdoutos, E., Daniel, I.M. and Wang, K. (2002), "Indentation failure in composite sandwich structures", *Exp. Mech.*, **42**(4), 426-431. https://doi.org/10.1007/BF02412148.

George, A., Shah, P.A. and Shrivastav, P.S. (2019), "Natural biodegradable polymers-based nano-formulations for drug delivery: A review", *Int. J. Pharm.*, **561**, 244-264. https://doi.org/10.1016/j.ijpharm.2019.03.011.

Ghorbanpour-Arani, A., Mosayyebi, M., Kolahdouzan, F., Kolahchi, R. and Jamali, M. (2017), "Refined zigzag theory for vibration analysis of viscoelastic functionally graded carbon nanotube reinforced composite microplates integrated with piezoelectric layers", *Proc. Inst. Mech. Eng. G J. Aerosp. Eng.*, **231**(13), 2464-2478. https://doi.org/10.1177/0954410016667150.

Ghorbanpour-Arani, A., Kolahdouzan, F. and Abdollahian, M. (2018), "Nonlocal buckling of embedded magnetoelectroelastic sandwich nanoplate using refined zigzag theory", *Appl. Math. Mech.*, **39**(4), 529-546. https://doi.org/10.1007/s10483-018-2319-8.

Guo, Y., Jiang, Y. and Huang, B. (2019), "Independent coordinate coupling method for vibration analysis of a functionally graded carbon nanotube–reinforced plate with central hole", *Adv. Mech. Eng.*, **11**(8), 1687814019872924. https://doi.org/10.1177/1687814019872924.

Hajmohammad, M.H., Sharif Zarei, M., Farrokhian, A. and Kolahchi, R. (2018), "A layerwise theory for buckling analysis of truncated conical shells reinforced by CNTs and carbon fibers integrated with piezoelectric layers in hygrothermal environment", *Adv. Nano Res., Int. J.*, **6**(4), 299-321. https://doi.org/10.12989/anr.2018.6.4.299.

Herrmann, A.S., Zahlen, P.C. and Zuardy, I. (2005), *Sandwich Structures 7: Advancing with Sandwich Structures and Materials, Springer*, Aalborg, Denmark.

Hosseini Hashemi, S.H., Es'haghi, M. and Karimi, M. (2010), "Closed-form vibration analysis of thick annular functionally graded plates with integrated piezoelectric layers", *Int. J. Mech. Sci.*, **52**(3), 410-428. https://doi.org/10.1016/j.ijmecsci.2009.10.016.

Karami, B., Janghorban, M. and Tounsi, A. (2018), "Galerkin's approach for buckling analysis of functionally graded anisotropic nanoplates/different boundary conditions", *Eng. Comput.*, **2018**, 1-20. https://doi.org/10.1007/s00366-018-0664-9.

Katariya, P.V., Panda, S.K., Hirwani, C.K., Mehar, K. and Thakare, O. (2017), "Enhancement of thermal buckling strength of laminated sandwich composite panel structure embedded with shape memory alloy fibre", *Smart Struct. Syst., Int. J.*, **20**(5), 595-605. https://doi.org/10.12989/sss.2017.20.5.595.

Ke, L.L., Liu, C. and Wang, Y.S. (2015), "Free vibration of nonlocal piezoelectric nanoplates under various boundary conditions", *Physica E Low Dimens. Syst. Nanostruct.*, **66**, 93-106. https://doi.org/10.1016/j.physe.2014.10.002.

Kiani, Y. (2017), "Dynamics of FG-CNT reinforced composite cylindrical panel subjected to moving load", *Thin-Wall. Struct.*, **111**, 48-57. https://doi.org/10.1016/j.tws.2016.11.011.

Lei, Z., Liew, K.M. and Yu, J. (2013), "Buckling analysis of functionally graded carbon nanotube-reinforced composite plates using the element-free kp-Ritz method", *Compos. Struct.*, **98**, 160-168. https://doi.org/10.1016/j.compstruct.2012.11.006.

Malekzadeh, P. and Ouji, A. (2008), "Axisymmetric buckling analysis of laterally restrained thick annular plates using a hybrid numerical method", *Int. J. Press. Vessel. Piping*, **85**(11), 789-797. https://doi.org/10.1016/j.ijpvp.2008.07.001.

Mehar, K. and Kumar Panda, S. (2018), "Thermal free vibration behavior of FG-CNT reinforced sandwich curved panel using finite element method", *Polym. Compos.*, **39**(8), 2751-2764. https://doi.org/10.1002/pc.24266.

Mehar, K., Kumar Panda, S. and Mahapatra, T.R. (2017), "Thermoelastic nonlinear frequency analysis of CNT reinforced functionally graded sandwich structure", *Eur. J. Mech. A Solids*, **65**, 384-396. https://doi.org/10.1016/j.euromechsol.2017.05.005.

Motezaker, M. and Eyvazian, A. (2020), "Post-buckling analysis of Mindlin Cut out-plate reinforced by FG-CNTs", *Steel Compos. Struct., Int. J.*, **34**(2), 289-297. https://doi.org/10.12989/scs.2020.34.2.289.

Motezaker, M., Jamali, M. and Kolahchi, R. (2020), "Application of differential cubature method for nonlocal vibration, buckling and bending response of annular nanoplates integrated by piezoelectric layers based on surface-higher order nonlocal-piezoelasticity theory", *J. Comput. Appl. Math.*, **369**, 112625. https://doi.org/10.1016/j.cam.2019.112625.

Panda, S. and Singh, B. (2009), "Thermal post-buckling behaviour of laminated composite cylindrical/hyperboloid shallow shell panel using nonlinear finite element method", *Compos. Struct.*, **91**(3), 366-374. https://doi.org/10.1016/j.compstruct.2009.06.004.

Reddy, J.N. (1984), "A simple higher-order theory for laminated

composite plates", *J. Appl. Mech.*, **51**(4), 745-752. https://doi.org/10.1115/1.3167719.

Shen, H.S. (2009), "Nonlinear bending of functionally graded carbon nanotube-reinforced composite plates in thermal environments", *Compos. Struct.*, **91**(1), 9-19. https://doi.org/10.1016/j.compstruct.2009.04.026.

Talebitooti, M. (2013), "Three-dimensional free vibration analysis of rotating laminated conical shells: Layerwise differential quadrature (LW-DQ) method", *Arch. Appl. Mech.*, **83**(5), 765-781. https://doi.org/10.1007/s00419-012-0716-3.

Thai, H.T. and Vo, T.P. (2012), "A nonlocal sinusoidal shear deformation beam theory with application to bending, buckling, and vibration of nanobeams", *Int. J. Eng. Sci.*, **54**, 58-66. https://doi.org/10.1016/j.ijengsci.2012.01.009.

Van Vuure, A.W., Ivens, J. and Verpoest, I. (2000), "Mechanical properties of composite panels based on woven sandwich-fabric preforms", *Compos. Part A Appl. Sci. Manuf.*, **31**(7), 671-680. https://doi.org/10.1016/S1359-835X(00)00017-8.

Vinson, J.R. (1999), *The Behavior of Sandwich Structures of Isotropic and Composite Materials*, CRC Press, Pennsylvania, USA.

Wang, M., Li, Z.M. and Qiao, P. (2016), "Semi-analytical solutions to buckling and free vibration analysis of carbon nanotube-reinforced composite thin plates", *Compos. Struct.*, **144**, 33-43. https://doi.org/10.1016/j.compstruct.2016.02.025.

Yue, X., He, W., Meng, T. and Song, Y. (2019), "Vibration control and stability analysis of a nanobeam with boundary prescribed performance", *Int. J. Control*, **2019**, 1-10. https://doi.org/10.1080/00207179.2019.1629026.

Zhang, L., Song, Z. and Liew, K. (2015), "Nonlinear bending analysis of FG-CNT reinforced composite thick plates resting on Pasternak foundations using the element-free IMLS-Ritz method", *Compos. Struct.*, **128**, 165-175. https://doi.org/10.1016/j.compstruct.2015.03.011.

CC